Nanotechnology **20** (2009) 235703 (9pp) doi:10.1088/0957-4484/20/23/235703

Size effects in nanoindentation of hard and soft surfaces

Michele Alderighi[1], Vincenzo Ierardi[1], Francesco Fuso[2], Maria Allegrini[2] and Roberto Solaro[1]

[1] Department of Chemistry and Industrial Chemistry, University of Pisa, Via Risorgimento 35, 56126 Pisa, Italy
[2] CNISM and Department of Physics Enrico Fermi, University of Pisa, Largo Bruno Pontecorvo 3, 56127 Pisa, Italy

Received 4 February 2009, in final form 31 March 2009
Published 19 May 2009
Online at stacks.iop.org/Nano/20/235703

Abstract
Nanoindentation experiments carried out with atomic force microscopes (AFMs) open the way to understand size-related mechanical effects that are not present at the macro- or micro-scale. Several issues, currently the subject of a wide and open debate, must be carefully considered in order to measure quantities and retrieve trends genuinely associated with the material behaviour. The shape of the nanoindenter (the AFM tip) is crucial for a correct data analysis; we have recently developed a simple geometrical model to properly describe the tip effect in the nanoindentation process. Here, we demonstrate that this model is valid in indentation of both soft and hard, or relatively hard, materials carried out by two distinct, commercially available, AFM probes. Moreover, we implement the model with a data interpretation approach aimed at preventing underestimation of the tip penetration into the material. Experiments on soft polymeric materials (poly(methyl methacrylate) and polystyrene) and hard or relatively hard (Si, Au, Al) materials are reported. The results demonstrate that true hardness data can be attained also in shallow indentations and that the appearance of size effects strongly depends on data interpretation issues. In addition, we report on stiffness data measured on the considered materials during their nanoindentation.

(Some figures in this article are in colour only in the electronic version)

1. Introduction

Investigation of hardness is of paramount importance for any application involving mechanical properties of materials. Measurement of hardness H at the macroscopic scale is straightforward [1]: a known load is applied onto the material surface by a specifically shaped indenter and hardness is related to the maximum applied load P_{MAX} according to

$$H = \frac{P_{MAX}}{A_C}, \tag{1}$$

where the indented area A_C is evaluated by direct optical imaging of the mark left on the surface.

Transferring such a simple procedure to the nanometre scale, meaning the ability both to measure effects produced by nanometric indentations and to analyse heterogeneous systems and thin films, is hampered due to the cumbersome evaluation of A_C. In fact, direct optical imaging fails due to diffraction effects. Based on the work by Oliver and Pharr [2] and on the original calculations introduced by Sneddon [3], nanoindentation, also known as depth sensing indentation (DSI [4]), was introduced to overcome such difficulties. The technique is based on continuously measuring the vertical displacement of a hard nanosized indenter against the material surface under application of a variable load. Neglecting higher orders in the approximation, the contact area can be expressed as a function of the penetration depth h of the indenter measured at the maximum load:

$$A_C \propto C_{tip} h^m, \tag{2}$$

where both C_{tip} and the coefficient m depend on the actual indenter geometry. Besides dedicated DSI instrumentation, atomic force microscopes (AFMs) have been used to study the mechanical response of surfaces [5–11] using the tip as a nanoindenter and exploiting the instrumental ability to acquire force–distance curves.

Nanoindentation enabled investigations entailing loads as small as tenths of a micronewton and depths as small as a

few nanometres. Important issues arise when the interplay between elasticity and plasticity is studied at a size comparable to the scales relevant to material microstructure [12–15]: nanoindentation results are often in disagreement with those acquired by conventional (macroscopic) techniques, opening the door to a variety of interpretations. For instance, strain gradients produced in the small indentation volume can lead to an increase of hardness at small penetration [16, 17], typically obeying an inverse power-law as a function of the depth, further followed by a decrease at even smaller depths, which has been explained as a sort of dislocation starvation at the local scale [16, 18].

A wide debate is still open as to whether those size effects have to be fully attributed to the material behaviour at the nanoscale (intrinsic size effect, see for instance [19, 20]), or they can be explained in terms of instrumental behaviour [14, 21–23]. There are at least two main reasons, which can lead to instrumental artefacts, related to the description of the indenter geometry and the evaluation of the quantities relevant to the tip penetration into the surface, respectively.

We recently developed a geometrical model to accurately describe the shape of AFM probes used as nanoindenters, which was applied to measure the hardness of a commercial WC/C alloy used in wear-protective coatings [24]. The main goals of the present paper are to implement the model with a data interpretation approach aimed at deriving genuine tip penetration depths and to apply it to a variety of materials, including soft matter such as, polystyrene (PS) and poly(methyl methacrylate) (PMMA) films, as well as harder polycrystalline (gold, aluminium, silicon) samples. Commercial instrumentation and two distinct AFM probes were used. In addition to hardness, contact stiffness S, defined as the resistance of an elastic body to deflection by an applied force, is also calculated for all investigated samples as the unloading rate during load removal [2]. The results demonstrate that size effects can be suppressed, at least partially, when proper data interpretation methods are used.

2. Experimental details

A commercially available microscope (Multimode with Nanoscope IV controller, Veeco Instr. Santa Barbara Ca.), equipped with a PicoForce stage allowing for closed-loop scans in the Z direction and a J-type scanner, was used. A digital oscilloscope connected to a signal access module served to collect signals representative of piezo displacement (both vertical and lateral) and cantilever deflection. This provided an additional check of the time resolved behaviour of the instrument, useful for instance to verify the occurrence of purely vertical deflections of the cantilever during the indentation and to measure the time spent by the system in applying the maximum load to the sample surface. Either commercially available diamond-coated or pure diamond tips (DDESP and DNISP probes from Veeco Instr.) were chosen as nanosized indenters for relatively soft and hard materials, respectively.

A proper description of the tip geometry is one of the key points of our approach. The DDESP tip is made of antimony-doped silicon coated by a diamond film (∼100 nm thick); it presents an anisotropic shape (rhomboidal), the height being ∼18 μm. This tip is mounted on a relatively high elastic constant cantilever (∼42 N m^{-1}) with a length of 125 μm and a width of 30 μm. The DNISP is a hand crafted ultra high force AFM probe specifically conceived for nanoindenting applications and fabricated by precision grinding a diamond having a triangular equilateral pyramid shape. The diamond is glued directly onto a stainless steel cantilever with an elastic constant of slightly below 224 N m^{-1} (data provided by the manufacturer), a value large enough to produce strong loads even at very small deflections (few tens or hundreds of nanometres) typical of AFM experiments. Due to the quasi-static nature of the indentation process, the damping coefficient of the steel cantilever, larger than for silicon-based probes, is expected to play a negligible role in the measurements.

3. Tip model and data analysis

The extent of tip penetration into the material can be determined by analysing the force–distance curves acquired during the vertical displacement of the sample against the tip [2]. A geometrical model specifically tailored to the used indenter (tip) is then needed for correctly describing the contact area.

According to the manufacturer, the vertex angles of the rhomboidal DDESP tip are 15° and 25° for the front and back faces, respectively. The side angle is 17.5° and the nominal radius of the apical curvature is around 15–20 nm. The DNISP tip has an equilateral pyramidal shape with a nominal 30° angle at the edge. The curvature radius at the apex is about 40 nm. We studied the actual tip shapes by performing tip reconstruction experiments that allowed for a very detailed evaluation of the apical radius. Moreover, since the apical shape can be obviously affected by wearing, tip reconstruction experiments were repeated before and after a measurement session to assess the tip bluntness. A test grating sample (TGT1 from NT–MDT Zelenograd, Moscow, Russia) comprising a regular array of sharp spikes with well-known geometry (3 μm period, 50° angle, apical radius $<$ 10 nm) was imaged to this aim. The AFM topography map normally given by convolution of tip plus sample shape, for extremely sharp sample features is representative of the tip morphology [25]. As an example, figure 1 shows the (inverted) image of DDESP (a) and DNISP tips (b) obtained in non-contact mode scans of the test grating sample. From scans at different magnifications we could derive the tip angle values, which turned out to be somewhat different (typically, within 30%) from the manufacturer specifications. Moreover, the apical radius R derived from high-resolution scans of the test grating can appreciably differ from the nominal value. For the tips used in this work, we measured $R \sim 20$ and 80 nm for DDESP and DNISP probes, respectively.

Due to the quasi-spherical shape of the apex, the indenter can be considered almost spherical when the indentation depth is below a certain threshold, whereas a pyramidal or

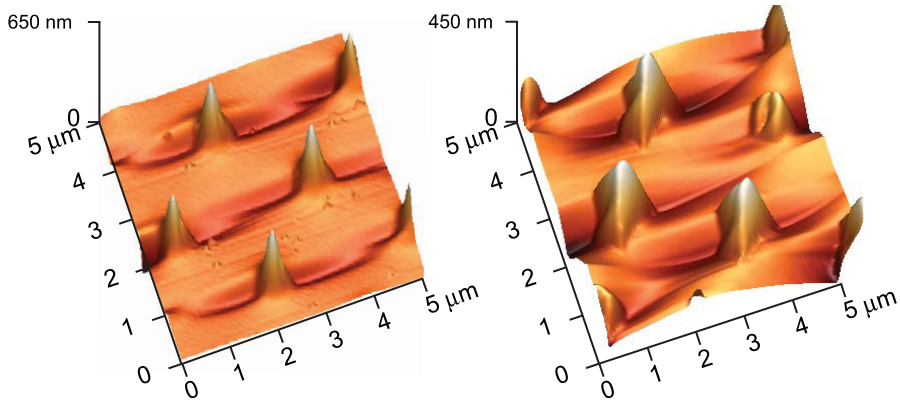

Figure 1. AFM topography of the spike grating sample acquired in non-contact mode with DDESP (a) and DNISP (b) tips. Due to the smallness and sharpness of the spikes, the images represent the inverted shape of the tips.

rhomboidal shape is predominant at larger indentation values. As a consequence, the dependence of the projected area on the indentation depth acquires a different behaviour at increasing depths. In our model [24] we calculate the projected area as a function of the indentation depth by means of geometrical rules based on the actual measured values of the apical radius and of the relevant angles. Furthermore, the model accounts for the geometry of the probe holder. In our set-up the displacement of the tip is tilted by a fixed value (12°) with respect to the vertical direction. Such a value can be modified by the instrument controller, which then imposes an adjustment of the in-plane position during the vertical displacement, but any modifications to the default value may lead to an erratic behaviour and to non-reproducible results. In order to duly recover the presence of the quasi-spherical apex, our model considers a smooth transition from the spherical to the pyramidal shape by assuming parallel surfaces in the transition region. Such a transition occurs near an effective radius R_{eff} that depends on the actual apical radius R according to:

$$R_{\mathrm{eff}} = R(1 - \sin\alpha), \tag{3}$$

with α being the angle at the vertex of the tip measured through the tip reconstruction experiment.

Figure 2 shows the dependence of the projected area on the indentation depth predicted by the model for both used tips. The DDESP is much sharper than the DNISP tip, leading to a slower increase of the contact area at increasing indentation depths. Therefore, the transition from the spherical to the pyramidal regime (taking place around $R_{\mathrm{eff}} = 20$ and 13 nm, respectively) is much more clear for DNISP than for DDESP.

Once the relationship between depth and area has been established, the indentation depth can be evaluated from the force–distance curves, hence providing the contact area. Figure 3(a) shows a typical curve acquired during indentation of a gold sample. The vertical axis is scaled in units of force after calibration of the instrumental sensitivity, which depends on the response of the deflection detector, calibrated through imaging hard reference grids and on the cantilever stiffness. The spring constant of the cantilever was taken from the manufacturer specifications. The zero of the axis is set at the piezo displacement corresponding to tip–surface contact.

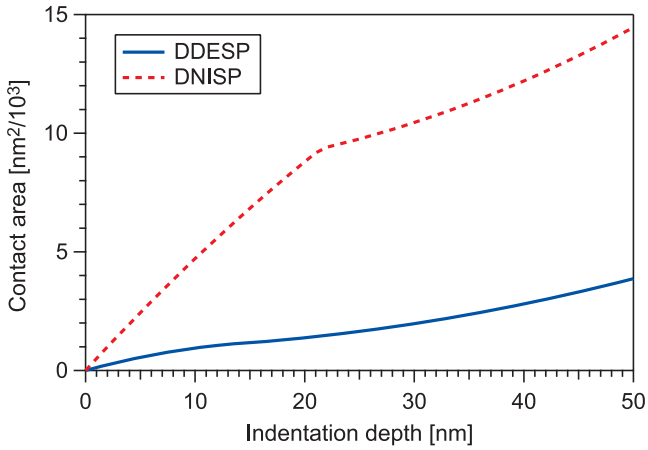

Figure 2. Contact area as a function of the indentation depth calculated according to our geometrical model for DDESP and DNISP tips.

During the loading stage, the force exerted by the tip on the sample surface is steadily increased up to a maximum value. It is worth noting that in AFM-based nanoindentation the applied force is inherently proportional (at the first approximation) to the cantilever deflection through its elastic constant [26]. After application of the maximum load, the piezo is retracted (unloading) and the cantilever deflection decreases until the tip is again completely disengaged from the surface.

Evaluation of the maximum applied force P_{MAX} is rather straightforward, whereas the procedure to identify the indentation depth deserves more comments. In particular, two different quantities can be defined, denoted hereafter as the final indentation depth (h_{F}) and the contact depth (h_{C}), respectively. h_{F} can be easily derived as the distance between the piezo position corresponding to the start of the loading and the end of the unloading curve. Considering such a measurement as truly representative of the tip penetration can fail to account for the surface behaviour during application of the load. The material can undergo either pile-up or sink-in effects [27]. In the first case, material is displaced from the centre towards the borders of the indented region, where

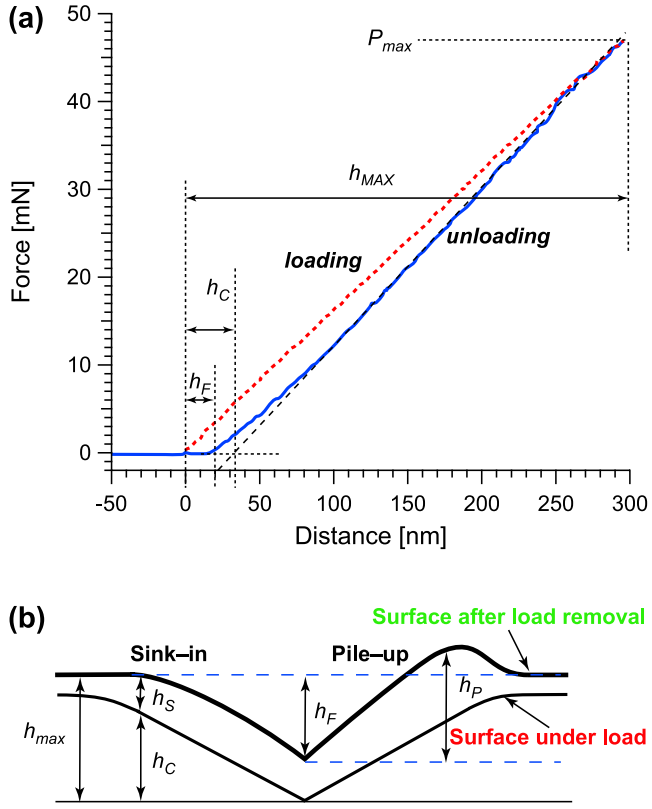

Figure 3. Example of a force–distance curve acquired by nanoindentation of the reference gold sample (a); pictorial representation of the involved depths (b), as discussed in the text.

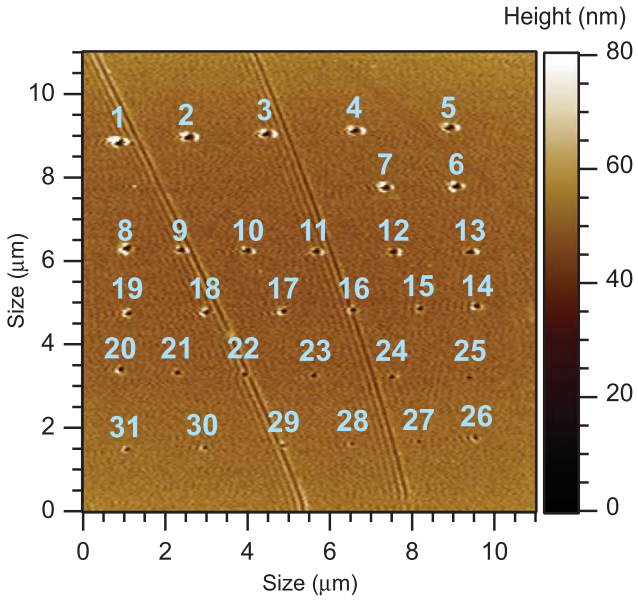

Figure 4. Indentation array performed on the surface of the gold reference sample. Marks 1–7 were produced without any delay between loading and unloading, whereas marks 8–31 were produced by applying the maximum load for 2 s. The AFM topography was acquired in the contact mode.

an artificial hill appears at the end of the indentation process (see, e.g., the pictorial representation in figure 3(b)). Such a protrusion can affect the evaluation of the indentation depth by raising the tip position at the end of the unloading process, leading to an overestimated value, h_P in figure 3(b). In the sink-in process, material is displaced towards the direction parallel to the surface plane because the load is not perfectly perpendicular to the material surface. Thus, sink-in involves material flow along the surface, ruled by elasto-plastic and viscous mechanisms. Because of this effect, the profile of the indented region does not fully reproduce the indenter shape and a sink-in depth, h_S, can be identified, as sketched in figure 3(b).

According to the literature [2, 28, 29], the contact depth, i.e., the penetration actually achieved during the application of load, can be derived by linear interpolation of the initial part of the unloading curve, where the contribution of plastic deformations, including those leading to pile-up, is negligible. The intersection of the linear interpolation with the horizontal axis identifies h_C.

In the measurements reported in section 4 we have systematically used both h_F and h_C values to feed our geometrical model, hence to derive the contact area A_C and the associated hardness H for all investigated samples. The main aim is to point out the effects on the evaluation of H and on its behaviour as a function of the penetration depth associated with the use of h_F or h_C for materials showing different mechanical properties.

4. Nanoindentation of the reference sample

A relatively flat (average roughness $\sim$ 6 nm over a 5 μm^2 area) gold layer was chosen as the reference sample for the indentation measurements. It is a commercially available polycrystalline gold film (average grain size 50–80 nm) deposited by evaporation onto silicon by interposing a 10 nm chromium adhesion layer. The gold layer thickness (200 nm) is much larger than the typical indentation depth achieved in our experiments, thus making negligible any possible contribution of the underlying layers [30]. Figure 4 shows an array of 31 indentation marks produced on the surface at predefined positions by using the DNISP tip: the image was obtained in contact mode right after the indentation process. All marks were numbered and a comprehensive analysis of the corresponding force–distance curves was carried out.

All marks in figure 4 were produced by setting a constant vertical displacement speed of 200 nm s^{-1}. However, indentation marks numbered from 1 to 7 were obtained with no delay between loading and unloading, whereas for the remaining marks the tip was left in contact with the surface at the maximum applied load for a short time (2 s). Both imaging and analysis of force–distance curves did not provide any clear evidence of the role played by the prolonged maximum load application, at least for the small delay range considered in the experiment.

Analysis of figure 4 suggests that the indentation depth is not constant even in marks belonging to the same category (i.e., with or without prolonged application of the maximum load). A possible explanation is as follows: all marks were produced imposing a constant piezo sweep range, with no control on the initial tip–sample distance. As a consequence, the maximum applied load was not the same for all indentations, resulting in

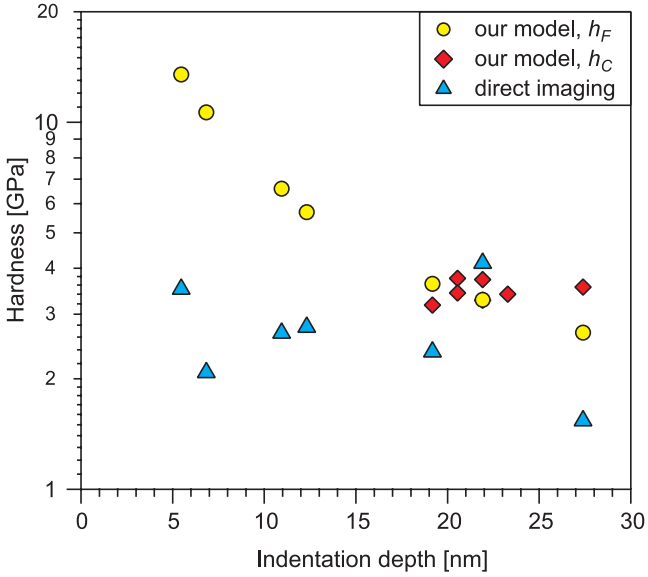

Figure 5. Gold hardness evaluated by nanoindentation of the reference sample. Symbols correspond to different methods of evaluation, as specified in the legend and discussed in the text. Note the logarithmic scale of the vertical axis.

different effects. We note that the software of our instruments allows for predefining the maximum load (i.e., the maximum cantilever deflection) achieved in the indentation through the so-called triggered-mode, but we achieved non-reproducible results when using such an option, which was consequently avoided.

Owing to the ability of AFM in imaging the surface with nanometre spatial resolution, it is possible, although difficult, to directly evaluate the area of the indentation marks, which typically is a few tens of square nanometres. Hardness values thus computed (triangles in figure 5) consistently are in the 2–4 GPa range, independent of the indentation depth. Literature data report a gold hardness of about 1–1.2 GPa, whereas numerical simulations indicate slightly larger values for nanosized indentations [31]. Our data are thus in fair agreement with the expectations and the observed discrepancy is very likely attributable to underestimated contact area. In fact, processes such as, pile-up and sink-in, occurring during the load application, cannot be duly determined by imaging, i.e., analysed once the load has been removed. Furthermore, evaluation of the contact area is affected by a relatively large uncertainty, leading to relative errors above 15%.

More accurate data can be gained by analysing force–distance curves according to the approach described in section 3. Quite obviously, description of the tip geometry strongly affects the obtained results. For instance, by assuming a purely pyramidal shape, strongly overestimated hardness values (not reported in figure 5) are retrieved, accompanied by a markedly increasing trend at small penetration depths. The data obtained by using our geometrical model, implying a smooth transition from the spherical to the pyramidal shape, are in reasonable agreement with the expectations. However, different results are achieved depending on whether h_F or h_C are considered as representative of the tip penetration into the sample. In the first case (circles in figure 5), the hardness increases with decreasing indentation depth (note the logarithmic vertical axis in the plot). In particular, data for depths below 15 nm show an increasing trend that can be described by an inverse power-law dependence (power exponent $\sim$ 1.2 [24]); the asymptotic value of the fitting function at large indentation depths is in the hardness range reported in the literature for macroscopic measurements. On the contrary, the analysis carried out by considering h_C as representative of the penetration depth (diamonds in figure 5) leads to an almost complete suppression of the size effect. Hardness evaluated by this method is roughly constant in the explored range; however, its average value (3–4 GPa) is slightly larger than literature data.

We measured the hardness of another polycrystalline material, aluminium, indented by the DNISP tip. The sample, showing an average grain size 30–50 nm, has a polished surface with a residual roughness of about 10 nm over a 5 μm^2 area; due to exposure to air, its surface is expected to be coated by a thin oxide layer. Hardness of an aluminium sample depends on its microstructure and on its thermal and mechanical history, which, unfortunately, are not known for the investigated specimen. A macroscopic indentation test gave us a value in agreement with a literature data ($H \sim 1.6$ GPa [32]).

Figure 6(a) presents the comparison among aluminium hardness values obtained by using either h_F or h_C in the interpretation. Data scattering suggests sample heterogeneity: by repeating measurements at different surface positions, close each other, we usually recorded a slightly different behaviour. The occurrence of inhomogeneous surface oxidation might be involved in data scattering; however, we could not clearly identify any role of the oxide layer in our measurements. Results are typically in good agreement with the mentioned literature data, as indicated also by the relatively small range of hardness values encompassed in the vertical scale. No clear evidence of size effects can be detected: indeed, data scattering (within the small range of hardness measured) prevents any trend identification. Moreover, data obtained by using either h_F or h_C are quite consistent, suggesting that shape recovery effects at load removal are negligible in the case of our aluminium sample. We may speculate that the heterogeneous nature of the sample leads to a dislocation density large enough to allow for material accommodation even in the small volume concerned by the indentation. Contrarily to our observations, size effects were found to some extent in the investigation of a high purity polycrystalline aluminium specimen [33].

Silicon, another material we have considered in our measurements, is a highly ordered and hard material. The investigated sample consists of a piece of crystalline wafer (p-doped and {100} oriented) with a polished surface, which, due to storage in air, is coated by a thin ($\sim$2 nm) non-stoichiometric oxide film. Silicon hardness is relatively large (reference data are around 13 GPa [34]), which may indeed pose limitations to the reliability of our approach, since we cannot completely rule out residual deformations of the indenter. On the other hand, the large hardness of silicon allowed us to explore very shallow indentation regimes. We stress that the small displacements involved can be reliably recorded owing to the use of the closed-loop scanner of our AFM instrument.

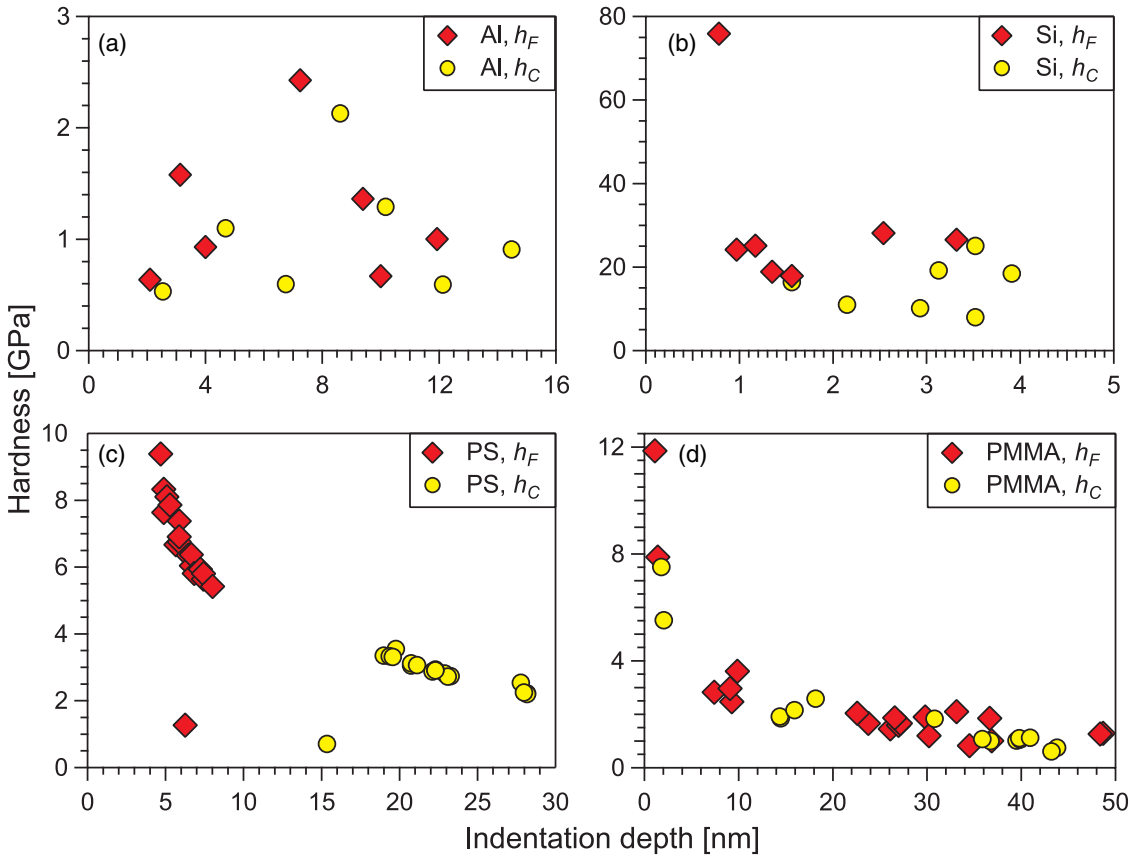

Figure 6. Hardness evaluated by nanoindentation of aluminium (a), silicon (b), polystyrene (c) and PMMA (d). Data are evaluated based on h_F (circles) or h_C (diamonds). Note that the plots have different horizontal and vertical scales, depending on the maximum indentation depths achieved in the experiments.

Results are shown in figure 6(b). Hardness evaluated on the basis of h_F is fairly constant for $h_F > 0.9$ nm, whereas the single data at $h_F \sim 0.7$ nm exhibits a very large hardness. It must also be noted that the obtained hardness is systematically larger than literature data. This result might indicate an underestimated penetration depth, for instance because of the sink-in effect. On the contrary, when h_C is used the computed hardness turns out to be in relatively good agreement with the literature. Moreover, size effects appear almost completely suppressed in this case. The native oxide layer was clearly also affected by our nanosized indentations. Even though its microstructure cannot be precisely determined and hence the associated hardness cannot be predicted (for reference, typical values for plasma-enhanced chemical vapour deposited oxides are around 9 GPa [29]), we may speculate that its occurrence is associated with the observed data scattering.

Soft materials investigated in the present work include polystyrene (PS) and poly(methyl methacrylate) (PMMA) films with estimated thicknesses in the hundreds of nanometres range. The films were produced on glass slides by spin coating at 5000 rpm a few drops of a polymer toluene solution. Because of the small material hardness, experiments were carried out by using the diamond-coated tip (DDESP), which gave us the opportunity to test our approach with a nanoindenter other than DNISP.

The value reported in the literature for polystyrene hardness is about 0.3 GPa [25]. As compared with inorganics, this organic material is also expected to show peculiar elasto-plastic behaviour due to its polymeric nature. In fact, indentation of soft matter can be affected by the inherently heterogeneous microstructure and its dynamics can be ruled by the distribution of the applied load within the polymeric matrix. Indentation at the nanoscale is thus expected to be a very powerful tool to ascertain the role of various phenomena occurring in the process. As a consequence, the issue of data interpretation may be even more relevant than in the case of harder (polycrystalline) materials.

Results are shown in figure 6(c): data interpreted by using h_F as the indentation depth show a marked increase at decreasing depth, with values consistently larger than literature data but for one single measurement. On the contrary, by representing the depth with h_C the size effect is much less prominent and the computed hardness tends to values more in agreement with conventional (macroscopic) measurements. More specifically, hardness evaluated by using h_C shows a residual decreasing trend at increasing depth, which gets an asymptotic value of 0.7 GPa when fitted by a power-law function, in fairly good agreement with the literature. We note however that we often observed space-dependent fluctuations, corresponding to harder and softer regions associated with local variations of the material microstructure that we could

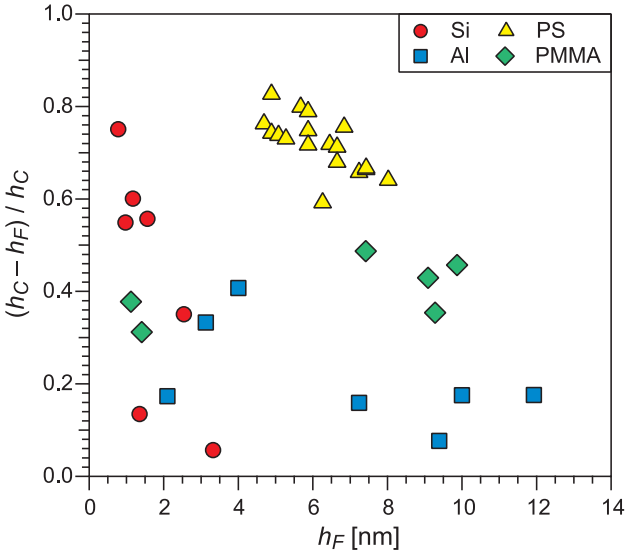

Figure 7. Normalized difference $(h_C - h_F)/h_C$ plotted against h_F for the investigated materials.

not relate to any clear surface morphology feature, such as the presence of defects or pits.

The value for the hardness of PMMA reported in the literature is about 0.4 GPa [35]. Our results presented in figure 6(d) are rather similar when using either h_F or h_C. It is worth noting the large range of explored penetration depths. In any case, observed hardness increase appears at indentation depths below 10 nm (for both h_F and h_C); asymptotic values attained by best fitting to a power-law function are in substantial agreement with the literature.

Comparison of PMMA with PS suggests that the mechanical behaviour of polymeric materials at the nanoscale strongly depends on their microstructure. Our data demonstrate remarkable differences between materials expected to behave similarly. We have not yet found a simple explanation for these findings that are very likely related to the specific dynamics of surface deformation upon load application in polymeric systems.

In summary, according to our analysis PS and, to a lesser extent, silicon data lead to an overestimate of both hardness and size effects when the indentation depth is represented by h_F. The statement is clarified in figure 7, where the normalized difference $(h_C - h_F)/h_C$ is plotted against h_F for the investigated materials. Such a difference provides a qualitative measure of effects, such as pile-up and sink-in, responsible for the erroneous evaluation of contact depth and hence of contact area. Our results demonstrate that those effects must be duly taken into account when performing nanosized indentations.

5. Elastic modulus

Along with hardness, force–distance curves recorded by AFM nanoindentation provide the contact stiffness, defined as the slope of the initial portion of the unloading curve [2]. Since plastic effects are expected to be negligible in the unloading stage, the contact stiffness is representative of the truly elastic response of the surface and hence it is related to the material elastic modulus. The mathematical formulation of such a relationship depends on the indenter shape; the following equation appears to hold true practically for all elastic contacts [36, 37]

$$S = 2E_{\text{eff}}\sqrt{\frac{A_C}{\pi}}, \tag{4}$$

where S is the measured stiffness and A_C is the contact area. A geometrical correction factor is often used as a multiplier in equation (4) to account for the actual geometry in conventional tests (e.g., those accomplished by Berkovich or corner-cube indenters). The presence of such a factor is in general questionable [37]; since our geometrical model is able to accurately describe the actual indenter shape, we did not use any further correction factor in our data analysis.

Indenter compliance issues must be carefully considered. As a matter of fact, the effective elastic modulus E_{eff} depends on the elastic modulus (E and E_{ind}) and Poisson's ratios (ν and ν_{ind}) of both the investigated material and the indenter, according to

$$\frac{1}{E_{\text{eff}}} = \frac{1-\nu_{\text{ind}}^2}{E_{\text{ind}}} + \frac{1-\nu^2}{E}. \tag{5}$$

Therefore, quantitative evaluation of the elastic modulus requires knowledge of indenter data and of the Poisson's ratio for the material under investigation, i.e., the ratio between transverse and axial strains. Such a knowledge cannot be achieved unless additional methods are used based for instance on the either microscopic investigations or numerical (finite elements) analysis.

The contribution of the indenter to the elastic strain is practically negligible, especially in the case of the diamond-made (DNISP) tip. Indeed, the literature elastic modulus and Poisson's ratio of diamond are above 1000 GPa and below 0.01, respectively [38]. Accordingly, the first term in the sum of equation (5) has a value of about 10^{-3} GPa^{-1}. Literature data do not allow a similar straightforward estimation of the compliance for the diamond-coated doped-silicon tip (DDESP). The elastic modulus of silicon is in fact much smaller than that of diamond (below 200 GPa [39]). However, the DDESP probe was employed only with materials having a much smaller elastic modulus; therefore, instrumental compliance is expected to be satisfied also in this case.

The effective elastic modulus E_{eff} as evaluated from indentation data is plotted against the contact depth h_C in figure 8. Our evaluation was limited to the effective modulus in order to avoid using reference data for the Poisson's ratio. In fact, most literature deals with conventional measurements for bulk specimens, which can differ from the situation entailed in our experiments. However, both the contribution of the indenter elasticity and the numerical modifications due to the Poisson's ratio are not expected to produce any dramatic change. The values presented in figure 8 are generally in good agreement with the literature data that are around 160 GPa for silicon [39] and 75 GPa for aluminium [40]. Values strongly dependent upon the specific sample features and in all cases

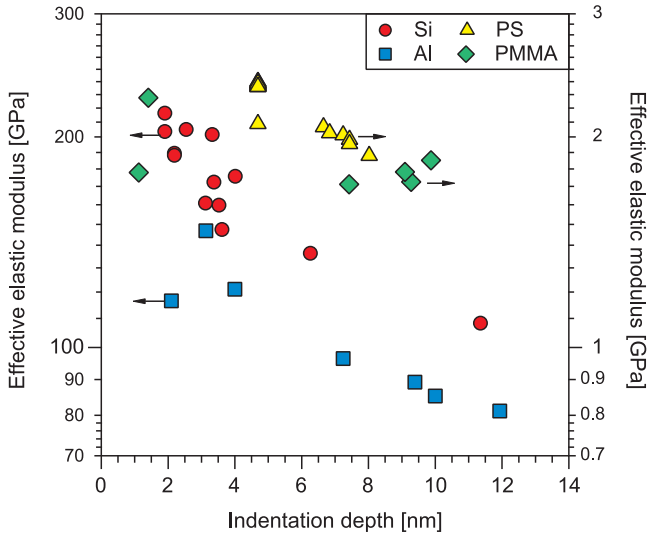

Figure 8. Effective elastic modulus evaluated for the investigated materials. All data refer to indentation depths in the range $h_C < 15$ nm. Note that the left axis corresponds to data for silicon and aluminium samples, whereas the right axis corresponds to data for polystyrene and PMMA.

in the range of a few GPa are reported for both PS [41] and PMMA [42].

Contact elasticity and hardness are ruled by tightly interconnected phenomena. They both represent the response of the surface to the applied load. In a rough picture, the elastic behaviour prevails at small loads below some threshold, whereas loads large enough to produce plastic yield lead to permanent (plastic) modifications. Thus, in both cases an accurate and reliable description of the contact area is required. Our data were acquired with indenters having two different geometries; therefore, the attainment of values in agreement with the literature further supports the validity of our approach in carrying out nanomechanical studies.

The data shown in figure 8 demonstrate a general increasing trend at small penetration depths, which can be roughly described with an inverse power-law function, the exponent being in the 0.1–0.2 range. Indentation at small depths implies application of the load mostly perpendicular to the sample surface, whereas an increasing fraction of shear forces is produced on the surface at increasing depths. As a consequence, the ratio between axial and parallel strains, conventionally expressed by the Poisson's ratio, turns out to depend on the extent of the penetration. Furthermore, already mentioned dislocations, voids and other defects can play a significant role in ruling the elastic response at the nanoscale as well as in determining the material hardness.

6. Conclusions

To investigate the nanomechanical properties of a variety of materials, we applied a geometrical model that accounts for the shape of AFM tips used as nanoindenters. Our results clearly demonstrate that there are issues to be carefully considered when measuring the mechanical response of a surface upon the application of small, highly localized loads, such as those attained in AFM-based nanoindentation. More specifically, besides description of the indenter geometry, which must be accurate enough to precisely evaluate the contact area as a function of the penetration depth, different results are obtained depending on whether the final or the contact depth is used to describe the tip penetration into the sample.

Interpretation of force–distance curves requires special care to prevent underestimates of phenomena involving material flow and rearrangement, such as sink-in and pile-up. These effects have been widely investigated in conventional (macroscopic) tests, but their role at the nanoscale is not yet fully clarified. There is evidence of a strong influence of the sample microstructure in ruling the mentioned effects. Further work is needed to interpret and to model such dependence.

Once cleared of instrumental artefacts, AFM-based nanoindentation can provide readily accessible data useful for a detailed nanomechanical analysis of both hard and soft materials. This information allows unravelling of size-related peculiarities in the response of surfaces upon application of small and highly localized loads.

Acknowledgments

Financial support by MIUR FIRB 2003 (research project RBLA03S4SP) and by Fondazione Cassa di Risparmio di Pisa (research projects PR/05/137 and PR/07/118) is gratefully acknowledged.

References

[1] Johnson K L 1987 *Contact Mechanics* (Cambridge: Cambridge University Press) pp 171–84
[2] Oliver W C and Pharr G M 1992 *J. Mater. Res.* **7** 1564
[3] Sneddon I N 1965 *Int. J. Eng. Sci.* **3** 47
[4] Doerner M F and Nix W D 1986 *J. Mater. Res.* **1** 601
[5] Drechsler D, Karbach A and Fuchs H 1999 *Acta Mater.* **47** 1043
[6] Kempf M, Goken M and Vehoff H 1998 *Appl. Phys.* A **66** S843
[7] Asif S A S, Wahl K J and Colton R J 2000 *J. Mater. Res.* **15** 546
[8] Grillo S E, Ducarroir M, Nadal M, Tournic E and Faurie J P 2003 *J. Phys. D: Appl. Phys.* **36** L5
[9] Garcia-Manyes S, Guell A G, Gorositza P and Sanz F 2005 *J. Chem. Phys.* **123** 114711
[10] Scholz T, McLaughlin K K, Giuliani F, Clegg W J, Espinoza-Beltran F J, Swain M V and Schneider F A 2007 *Appl. Phys. Lett.* **91** 62903
[11] Bushan B 2008 *Phil. Trans. R. Soc.* A **366** 1351
[12] Kiely J D, Hwang R Q and Houston J E 1998 *Phys. Rev. Lett.* **81** 4424
[13] Goken M, Kempf M and Nix W D 2001 *Acta Mater.* **49** 903
[14] Liu D L, Lu T M, Wang G C and Picu R C 2004 *Appl. Phys. Lett.* **85** 3053
[15] Wang F, Huang P and Xu K W 2007 *Appl. Phys. Lett.* **90** 161921
[16] Nix W D, Greer J R, Feng G and Lilleodden E T 2007 *Thin Solid Films* **515** 3152
[17] Huang Y, Xue Z, Gao H, Nix W D and Xia Z C 2000 *J. Mater. Res.* **15** 1786
[18] Greer J R, Oliver W C and Nix W D 2005 *Acta Mater.* **53** 1821
[19] Nix W D and Gao H 1998 *J. Mech. Phys. Solids* **46** 411
[20] Chong A C M and Lam D C C 1999 *J. Mater. Res.* **14** 4103

[21] Huang Y, Zhang F, Hwang K C, Nix W D, Pharr G M and Feng G 2006 *J. Mech. Phys. Solids* **54** 1668
[22] Chen W, Li M, Zhang T, Cheng Y T and Cheng C M 2007 *Mater. Sci. Eng.* A **445–6** 323
[23] Chicot D and Mercier D 2008 *Mech. Mater.* **40** 171
[24] Alderighi M, Ierardi V, Solaro R, Fuso F and Allegrini M 2008 *J. Nanosci. Nanotechnol.* **8** 1
[25] Bykov V A, Novikov Yu A, Rakov A V and Shikin S M 2003 *Ultramicroscopy* **96** 175
[26] Hutter J L 2005 *Langmuir* **21** 2630
[27] Mann A B 2005 *Nanotribology and Nanomechanics: An Introduction* ed B Bhushan (New York: Springer) pp 575–622
[28] Oliver W C and Pharr G M 2004 *J. Mater. Res.* **19** 3
[29] Zhiqiang C and Zhang X 2008 *Thin Solid Films* **516** 1941
[30] Kramer D F, Volinsky A A, Moody N R and Gerberich W W 2001 *J. Mater. Res.* **16** 3150
[31] Lee D, Wei X, Zhao M, Chen X, Jun S C, Hone J and Kysar J W 2007 *Modelling Simul. Mater. Sci. Eng.* **15** S181
[32] Saif M T A, Zhang S, Haque A and Hsia K J 2002 *Acta Mater.* **50** 2779
[33] Elmustafa A A and Stone D S 2002 *Acta Mater.* **50** 3641
[34] Bhushan B, Kulkarni A V, Bonin W and Wyrobek J T 1996 *Phil. Mag.* **74** 1117
[35] Berthoud P, G'Sell C and Hiver J M 1999 *J. Phys. D: Appl. Phys.* **32** 2923
[36] Kendall D and Tabor D 1971 *Proc. R. Soc.* A **323** 321
[37] Bhushan B 2004 *Springer Handbook of Nanotechnology* (Berlin: Springer) pp 661–86
[38] Telling R H, Pickard C J, Payne M C and Field J E 2000 *Phys. Rev. Lett.* **84** 5160
[39] Wortman J J and Evans R A 1965 *J. Appl. Phys.* **36** 153
[40] Lide D R (ed) 2001 *CRC Handbook of Chemistry and Physics* (Boca Raton, FL: CRC Press) pp 12-210–2
[41] Miyake K, Satomi N and Sasaki S 2006 *Appl. Phys. Lett.* **89** 031925
[42] Giddings V L, Kurtz S M, Jewett C W, Foulds J R and Edidin A A 2001 *Biomaterials* **22** 175